Okajimas Folia Anat. Jpn., **91**(3): 57–71, November, 2014

A histological study of mineralised tissue formation around implants with 3D culture of HMS0014 cells in Cellmatrix Type I-A collagen gel scaffold *in vitro*

By

Aiko MORISHITA, Shunji KUMABE, Michiko NAKATSUKA and Yasutomo IWAI

Department of Oral Anatomy, Osaka Dental University, 8-1 Kuzuhahanazono-cho, Hirakata-shi, Osaka 573-1121, Japan

–Received for Publication, November 25, 2014–

Key Words: Turn over, mesenchymal stem cells (MSCs), 3D collagen scaffold, GBR tissue

Summary: We cultured HMS0014 Yub621b cells within a 3D collagen gel scaffold (Cellmatrix Type I-A) and aimed to study the fate and contribution of human bone-derived mesenchymal stem cells (MSCs) in the guided bone regeneration(GBR)-engineered tissue which has developed around the titanium (Ti) test dental implant (IP) *in vitro*. The light microscopy (LM) and transmission electron microscopy (TEM) results of the peri-IP tissue indicated that collagen fibrils of the Cellmatrix Type I-A gel were accumulated and fabricated to provide a 3D meshwork for proliferation and differentiation of the HMS0014 cells in the top (cell) layer; mineralisation of the GBR tissue had commenced since day 1 and became markedly deposited between days 7 and 14 of the experiment. TEM observation revealed sedimentation of cement line at the periphery of the interwoven Cellmatrix fibres and fibrils in the ECM scaffold of the GBR tissue; matrix vesicle-mediated and appositional collagen-mediated mineralisation were identified in the peri-IP ECM scaffold. The fine structure study of the plurimorphic osteoblast(Ob)-like osteogeneic cells demonstrated numerous membranous organelles related with vesicular trafficking, secretion and endocytosis in the cytoplasm; well-developed cytoskeleton networks and intercellular junctional complexes were also observed. The specimens on fluorescence immunohistochemistry (IHC) by confocal laser-scanning microscopy (LSM) showed the expression of LC3 and Cx43 associated with autophagic-lysosomal degeneration pathway and signal conduction mediated with gap junctions (GJS) in maintaining tissue homeostasis of the Ob-like cells which grew and degenerated in the 3D scaffold. Results from this *in vitro* study suggest that Ob-like HMS0014 cells actively regulate turnover of the peri-IP ECM to recapitulate the development and formation of osteoid tissue-engineered material which might contribute to augment osseointegration around the dental implant.

Introduction

Many previous studies on osseointegration have elucidated that cell adhesion and proliferation were sensitive to substrate surface characteristics of dental implant (IP)s[1–11]. We have 3D-cultured JCRB1119:KUSA/A1 bone marrow-derived mesenchymal stem cell (MSC)s obtained from C3H/He mice (JCRB/HSRRB, Osaka, Japan) in a neutralised type I collagen gel (Cellmatrix Type I-A; Nitta Gelatin Inc., Osaka, Japan) with IPs, and observed hard tissue formation to mimic contact and the static osteogenesis in the GBR tissue surrounding titanium (Ti) IPs[2, 9, 12–19]. Recently, we have investigated initial contact osteogenesis of HMS0014 MSCs (Yub621b, human bone-derived MSC line; Riken BRC, Tsukuba, Japan) on Ti discs (plates) subject to different surface modifications. The study observed that HMS0014 cells differentiated into osteoblast(Ob)-like cells secreting abundant extracellular matrix (ECM) under induction condition, and mineralisation of the ECM was initiated since day 1 and thereby became markedly deposited on day 7 of the experiment. We therefore surmised that mineralisation was prominently and significantly progressed between days 7 and 14 under osteogeneic induction; more calcium (Ca) and osteocalcin (OC) volumes (in μg/μgDNA) were acquired in 3D cultures[10, 11]. Many studies have observed that immature MSCs (e.g., HMS0014 cells) were osteoinduced to migrate and attach onto the substrate of the Ti material surfaces subjected to modifications, and then differentiated into mature Ob-like cells which extended cell processes within 60 min of culture[2–4, 6, 10–12, 20–22]. Subsequently, the spherical-to-polygonal (diameter (d) = 10–40 μm) HMS0014 cells were differentiated into flat, large polyg-

Corresponding author: Shunji Kumabe, D.D.S., PhD., Dept. of Oral Anatomy, Osaka Dental University, 8-1 Kuzuhahanazono-cho, Hirakata-shi, Osaka 573-1121, Japan. E-mail: kumabe@cc.osaka-dent.ac.jp

onal (dimension = 30 μm × 90 μm to 100 μm × 200 μm) cells sending out prominent lamellipodia and filopodia within 180 min culture; we observed that the proliferating and differentiating Ob-like cells were more expansively adhered on the surface of anodic-oxidized (AO) Ti alloy discs. In addition, we demonstrated the expression and co-localisation of CD51 (the αv/β3 integrin: ITGAV, an interfacing specific receptor protein) and F-actin (filamentous actin cytoskeleton) in the matured Ob-like cells by immunohistochemistry (IHC) visualised using fluorescent microscopy[11].

There have some studies on GBR with osteogeneic cells seeded on 3D scaffolds that enhanced cell-biomaterial interactions to support growth and differentiation of cultured mesenchymal cells[9, 23–28]. As we have observed that the establishment of bone-to-implant direct contact (BIC) interfaces was initiated with attachment of pre-Obs which secreted non-collagen ECM proteins to enhance the sedimentation with a layer of calcified afibrillar cement line, and then the phenomenon was followed with additional crystal growth and collagen assembly to facilitate matricial mineralisation in the GBR peri-IP tissue to attain an appositional process of peri-IP contact osteogenesis[12–19, 29–31]. In the present *in vitro* study, we cultured HMS0014 Yub621b cells with anodic-oxidized Ti dental IPs (AO-IPs) in the Cellmatrix Type I-A gel that developed a substance essentially similar to the peri-IP tissue observed in our previous studies[9, 32]. We studied hard tissue formation in the tissue-engineering material mainly by transmission electron microscopy (TEM) and IHC by confocal laser-scanning microscopy (LSM) examination, aimed to reveal the fine structure and turnover of the osteoid tissue which might be utilised to offer augmentation of osseointegration tissue for dental IP therapy by the GBR concepts.

Materials and Methods

Immature HMS0014 : Yub621b (Human bone-derived mesenchymal, osteogeneic linage cells; Riken BRC) cells were filtrated, centrifuged and incubated/maintained in POWEREDBY10 (Glyco Technica Ltd., Sapporo, Japan) supplemented with 1% antibiotic-antimycotic agent (100 units/mL penicillin + 100 μg/mL streptomycin; Nacalai Tesque, Kyoto, Japan) in cell culture 75 cm^2 flasks (TPP, Switzerland) at 37°C in humid air with 5% CO_2 for 72h.

Tissue engineering of HMS0014 cells on Ti dental IPs

Primarily (finely-blasted) and secondarily (anodic-oxidized; AO) processed dental root-shaped and straight *α-β* type titanium alloy (Ti-6Al-4V) FINAFIX dental implants (d = 3.7 mm, l = 14.0 mm, POI system; KYOCERA Medical Co., Osaka, Japan; AO-IP) were laid in dishes paved with Cellmatrix Type I-A gel (base layer), cultured together with the cell cluster containing immature HMS0014 mesenchymal stem cells (MSCs) in Cellmatrix Type I-A collagen gel (top layer, cell layer), and overlaid with POWEREDBY10 (added with osteogeneic induction medium: ascorbic acid (AA) + *β*-glycerophosphate (*β*-GP) + dexametazone (DEX); overlay medium) hence the HMS0014 cells have been induced to different into mature osteogeneic osteoblast (Ob)-like cells on AO-IPs in a 3D microenvironment (1×10^6 cells/mL; humid 5% CO_2/37°C, for 21 days) since the day 3 of experiment according to the "Collagen Gel Embedded Culture Method" (http://www.nitta-gelatin.co.jp; Nitta Gelatin Inc.) to mimic osseointegration of AO-IPs in 10 cm dishes (IWAKI, Tokyo, Japan) under the induction condition *in vitro* (Fig. 1).

In contrast, HMS0014 MSCs 3D-cultured under non-inducing condition (without addition of the osteogeneic supplements) for 3 days following the same Collagen Gel Embedded Culture Method were prepared and designated to be the controls for the purpose of comparison with the experimentals (cultured under osteogeneic condition) in the present TEM study.

Histological studies

1. Light microscopy (LM)

Test IPs with surrounding mineralizing tissue (a visually opaque layer) were dissected from the cultures, fixed with 4% paraformaldehyde, dehydrated and embedded in Technovit 7200 VLC (Heraeus Kulzer GmbH & Co. KG, Wehrheim, Germany). The samples were sectioned with EXAKT BS-300CP-A Band Saw Machine and MG-400CS Microgrinding Machine (MEIWAFOSIS, Tokyo, Japan) by using the Cutting-Grinding Technique. Subsequently, the specimens were prepared for light microscopy (LM) study by an Olympus BX41 LM connected with a FX380 system (Olympus, Tokyo, Japan).

On the other hand, some of the dissected peri-IP tissue were immersion-prefixed (1/2 Karnovsky's fixatives), post-fixed (1.0% OsO_4), embedded in EPON 812 (TAAB, Berkshire, UK), trimmed and semithin sectioned with diamond knives on an ultratome (ULTROTOME; LKB, Stockholm, Sweden), and then prepared for LM survey specimens to select areas for the ultrathin sections.

2. Transmission electron microscopy (TEM)

The Epon 812 embedded specimens (the controls and experimentals) were ultrathin-sectioned with diamond knives using the ULTROTOME, picked up on copper grids, double electron stained (uranyl acetate and lead citrate), and then examined and photographed with a Hitachi H-7100 TEM (Hitachi, Tokyo, Japan).

3. Fluorescence immunohistochemistry (IHC) by confocal laser-scanning microscopy (LSM)

Some frozen-sectioned specimens subjected to acetone fixation were washed with PBS (5 min, 3 times), blocked

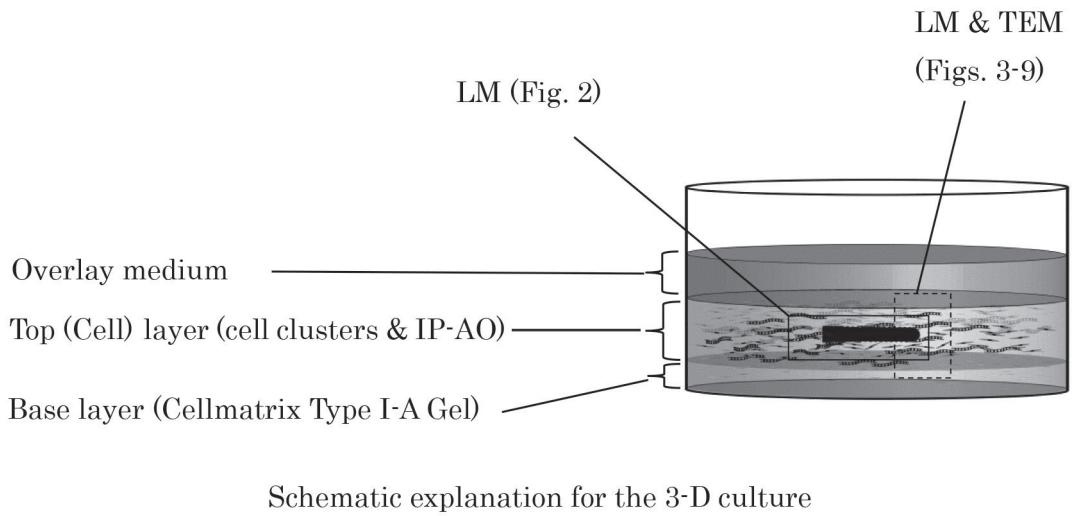

Fig. 1.

(10% NORMAL GOAT SERUM, 15 min; Vector Laboratories, Inc., Burlingame, CA, USA) and processed in the following methods:

1) Immunolocalisation of autophagosome formation in Ob-like cells:

Some specimens were washed and treated with anti-microtubule-associated protein 1 light chain 3 (anti-LC3) primary antibody (Anti-LC3, Rabbit-Poly Antibody; Novus Biologicals, LLC, Littleton, CO, USA; 1:400 dilution, 2h). After washing with PBS, the specimens were treated with Alexa Fluor 488 goat anti-rabbit IgG [H+L] (excitation wave length: 495 nm, fluorescence wavelength: 519 nm; Molecular Probes, Inc., Eugene, OR, USA; 1:400 dilution, 1h), and were washed with PBS again following the conventional methods.

2) Investigation of the gap junctions (GJS) related with signal conduction and turnover of Ob-like cells:

Other specimens were treated with NORMAL GOAT SERUM blocking solution, the specimens were reacted with primary antibody of Connexin 43 (Cx43) Antibody (Cell Signaling Technology, Inc., Danvers, MA, USA). After PBS washing, the specimens were stained with the Alexa Fluor 488 goat anti-rabbit IgG [H + L] secondary antibody and then washed again with PBS.

Subsequently, all the specimens for LC3 and Cx-43 immunolocalisation were treated with RNASE PANCREATIC (AMRESCO, Solon, OH, USA; 1mg/mL in PBS, 30 min) to denature the RNA in the tissue, washed with PBS and then counterstained with propidium iodide (PI) DNA stain (excitation wave length: 530 nm, fluorescence wavelength: 615 nm; Molecular Probes; 1.0mg/mL in distilled water, 30 min, room temp) to identify the cell nuclei. The double-stained specimens were PBS-washed, mounted in VECTASHIELD MOUNTING MEDIUM (Vector Laboratories) and examined with an Olympus personal LSM (OLYMPUS FLUOVIEW BX50; argon ion laser, excitation wavelength: 488 nm (CH1), filters: BA510F and BA530RIF; HeNe ion laser, excitation wavelength: 543 nm (CH2), filters: BA590 and BA565IF; Fluoview 2.0.32. Olympus).

Histological findings

We have performed preliminary studied of the peri-IP opaque tissue in the top/cell layer of the experimentals by LM and TEM. The LM of the grounded specimens (Fig. 2) and semithin sections (Fig. 3a) demonstrated adherence of osteogeneic induced-mesenchymal stem cell (MSC)s and sedimentation of cement line matrix on the IP-ECM interface and at the periphery of Cellmartix fibres that enhanced collagen-mediated mineralisation to initiate IP osteointegration by the contact osteogenesis phenomenon (Figs. 2 and 3a). In the top layer, the survey LM observed that many pleomorphic cells (dimension ≒ 10 μm × 70 μm) were widely dispersed in the ECM scaffold comprising many faintly stained fibrillar content and mineralisation loci (Fig. 3b). Furthermore, the TEM elucidated appositional mineralisation on the non-collagenous cement line of the ECM scaffold (Figs. 3c & 3d). Results of the preliminary experiment suggested that the ECM scaffold provided a 3D woven meshwork for the tissue-engineering procedure of culturing HMS0014 Ob-like cells within the Cellmatrix collagenous scaffold.

Hence, in the present study we conducted an investigation into the fate and contribution of the osteogeneic induced-HMS0014 bone-derived MSCs in the GBR-engineered tissue which has developed around the dental IP

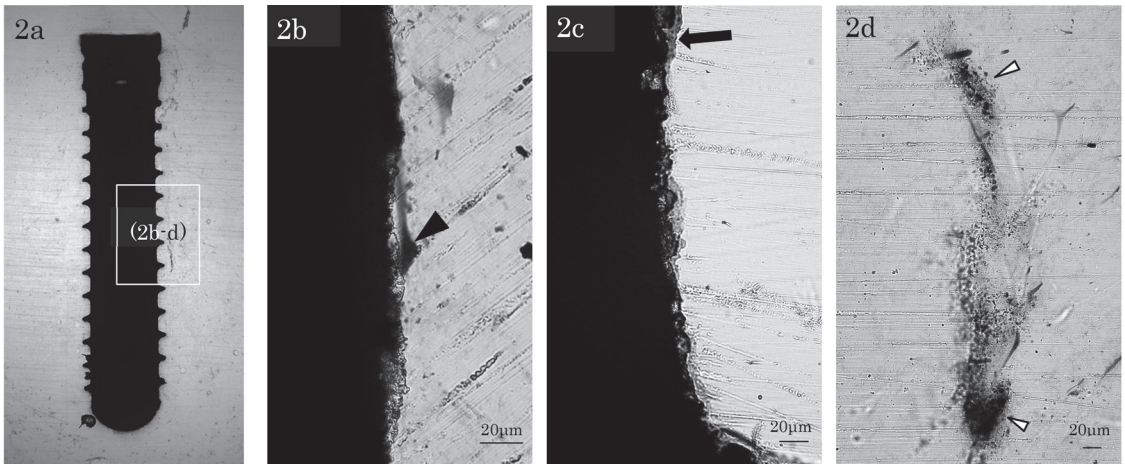

Fig. 2. LM of day 14 osseointegration *in vitro* (Olympus BX41/FX380 system). Fig. 2a LM of ground-sectioned AO-IP. High magnification of the peri-AO-IP tissue (Figs. 2b–d) shows attachment of Obs (▲), sedimentation of an afibrillar cement line (⬆), and collagen-related ECM mineralisation (△) to obtain a peri-IP osteogenesis.

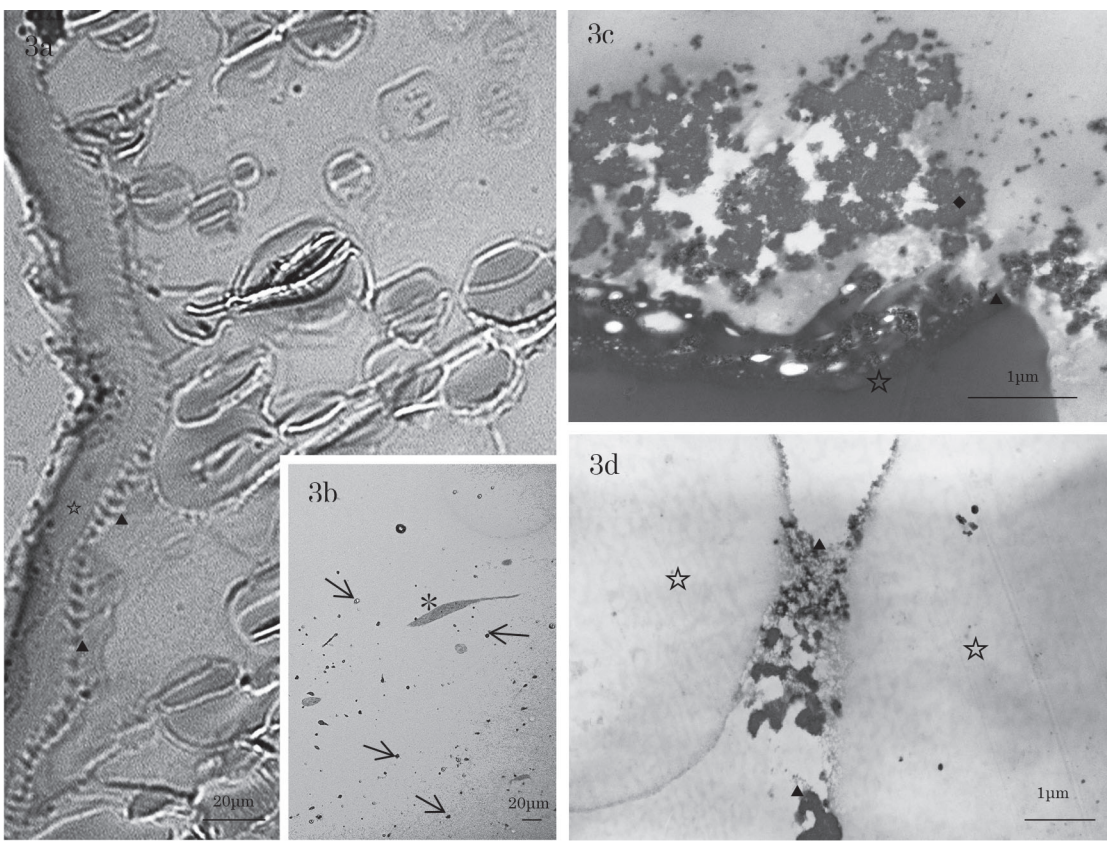

Fig. 3. Preliminary experimental study (day 21). Fig. 3a LM of a semithin section showing sedimentation of cement line matrix on the periphery of Cellmatrix scaffold (☆). Fig. 3b LM indicates that pleomorphic cells (∗) are widely dispersed in the ECM scaffold comprising many faintly stained fibrillar content and mineralisation loci (↑). Figs. 3c, d The TEM shows sedimentation of an afibrillar cement line (▲) at the periphery of Cellmatrix scaffold (☆) and collagen-mediated ECM mineralisation (◆), and therefore attains a direct osteogenesis of tissue-engineering tissue on the Cellmatrix Type I-A 3-D scaffold.

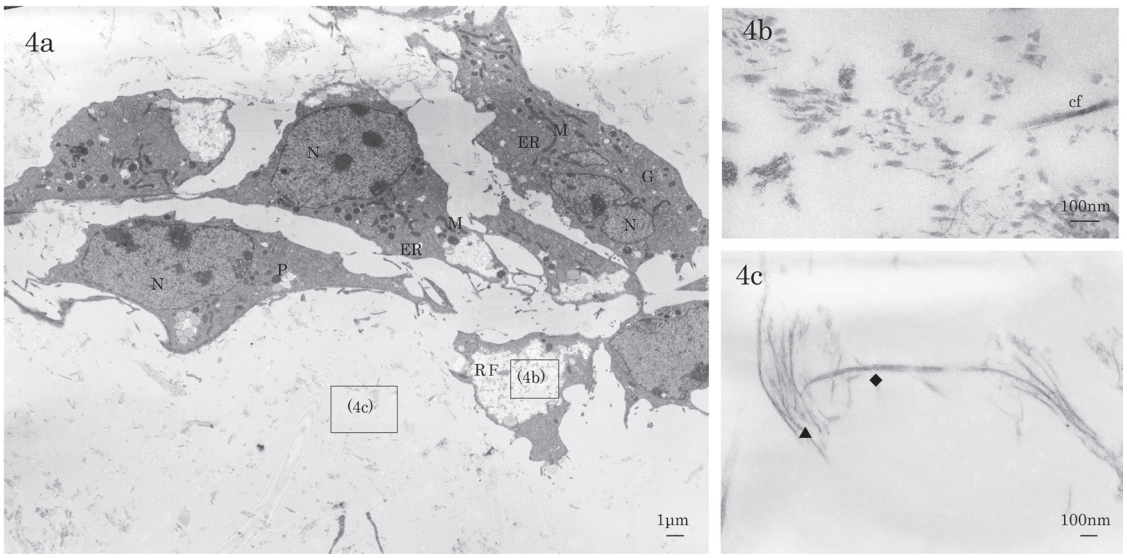

Fig. 4. TEM of the control group (day 3 controls). Fig. 4a The non-inducing HMS0014 cells are fibroblast-like MSCs with a high N/P ratio. The cytoplasm is rich in ribosomes, and consists of Golgi complexes (G), enlarged rER (ER), abundant mitochondria (M) and a few phagosomal lysosomes. Figs. 4a, b The MSCs are characterised by long and thin cell processes ensheathing the reticular fibre (RF) composed of thin collagen fibrils (cf) and amorphous materials. Fig. 4c TEM photogram showing Cellmatrix collagen fibrils (▲: thin fibrils, ◆: thick fibrils) in the ECM (day 3 control).

in vitro.

TEM of HMS0014 cells and the ECM in the cell layer

1. The control group (non-inducing cells 3D-cultured in type I collagen gel)

The dendritic spindle-shaped non-inducing MSCs were widely dispersed in the extracellular matrix (ECM). The cells extended pseudopodia-like structures, which further sent out many long and slender cytoplasmic processes characteristically ensheathing reticular fibres (diameter (d) = 1–3 μm) consisted of finely-scattered collagen fibrils (d ≒ 50 nm, indistinct band interval) and amorphous materials[33]; the cells were interconnected to make a cellular meshwork in the extracellular matrix (ECM) of the loose connective tissue structure (Figs. 4a & 4b).

The active MSCs contained an indented and ovoid-shaped nucleus finely distributed with hetero/eu chromatin, and the cells had a high nucleus-to-cytoplasm (N/P) ratio. The cytoplasm consisted of a small amount of Golgi complexes (the Golgi apparatus) and enlarged rough endoplasmic reticulum (rER) studded with electron dense material, abundant oval and elongated tubular mitochondria possessed dense matrices and distinct cristae, and a few phagosomal lysosomes; the cytosol was rich in ribosomes (Fig. 4a). We observed that the Cellmatrix collagen networks in the ECM were composed mainly of fine fibrils (d = 10 nm, band interval= indistinct) intermingled with a few thicker (d = 15–30 nm, band interval = 20 nm) fibrils (Fig. 4c).

The findings indicated that non-inducing MSCs 3D-cultured in Cellmatrix Type I-A gel (the controls) represented a more immature type of *in vitro* osteogenesis. The day 3 cells actively contributed to enhanced ECM formation, but no matrix vesicle (MV)- and collagen-mediated mineralisation of the ECM were found in the control specimens.

2. The experimental group (osteogeneic-induced cells 3D-cultured in Cellmatrix Type I-A collagen gel)

(1) Day 3 specimens:

The HMS0014 cells differentiated into Ob-like cells which showed a bulging cell body with extended, flat cytoplasm characteristically rich in lysosomes; the cells closely intercellularly junctioned (Fig. 5a). Many mitochondria in longitudinal and cross sections showed orthodox configuration with condensed matrix were observed in the cytoplasm (Figs. 5a, 5b & 5c). The TEM also demonstrated distribution of well-developed rER and Golgi apparatus, and small smooth-surface (d ≒ 150 nm) and coated vesicles (r ≒ 150–180 nm) nearby and at the cell membrane (Figs. 5a & 5b). Many vesicles were identified to be closely related with either lysosomes in the cytoplasm or nascent collagen of the ECM (Figs. 5a, 5b & 5c). These structures were organelles supporting the stable and maturation models for vesicular transport mechanisms concerning constitutive pinocytosis and secretion, as well as receptor-mediated endocytosis of the Ob-like cells.

On the other hand, at the vicinity to the plasma

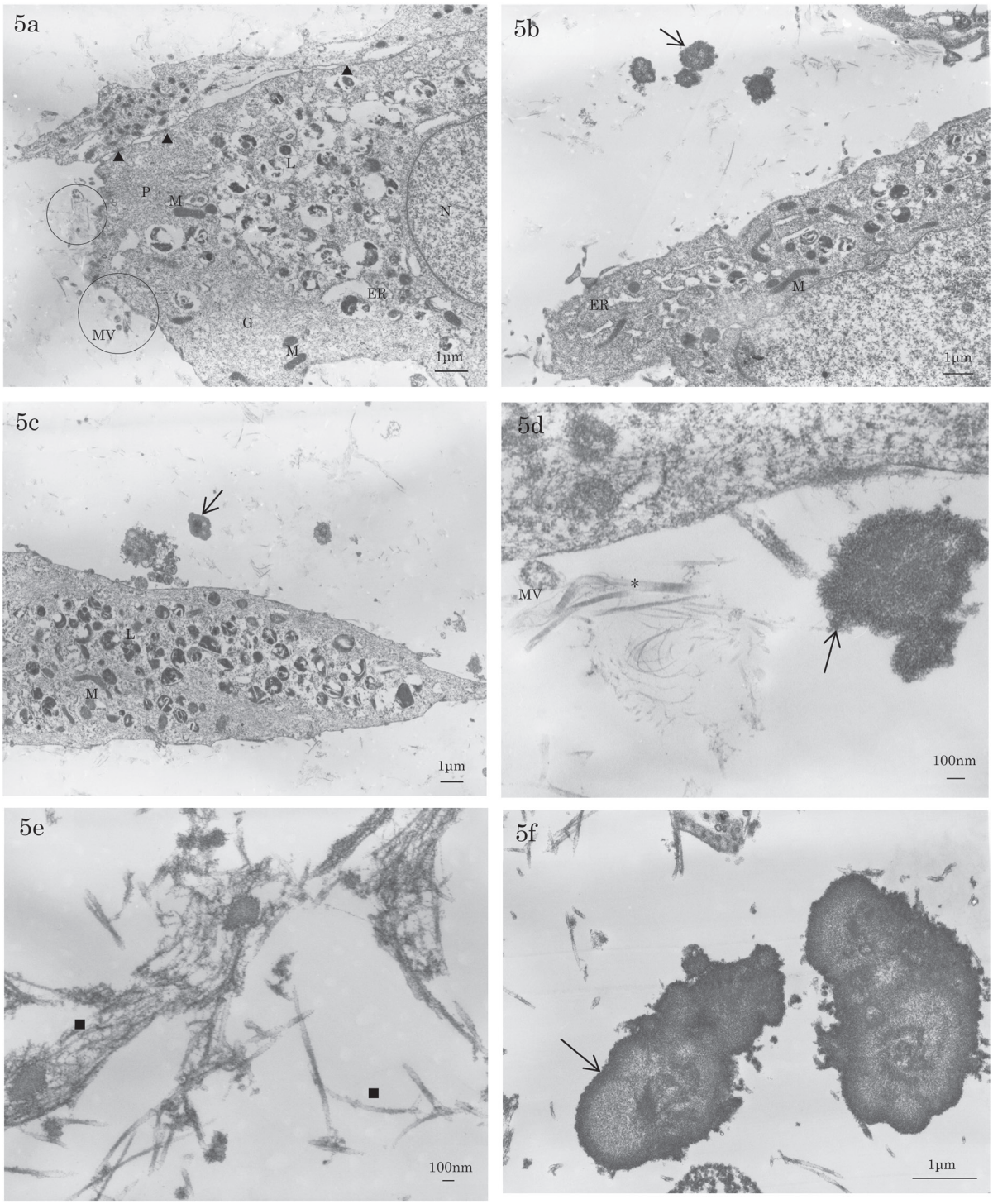

Fig. 5. TEM of the experimental group (day 3 experimentals). Fig. 5a The Ob-like cells have a bulging cell body showing low N/P ratio. The cytoplasm contains well-developed endoplasmic reticulum (ER) and Golgi apparatus (G), and many mitochondria (M). The cells are intercellularly junctioned (▲). Both matrix vesicle(MV)- and collagen-mediated mineralisation events are found at the periphery of Ob-like cells (circled areas). Fig. 5b The TEM shows an Ob-like cell and the ECM consisting of fibrils, calcospherite and mineralisation loci (↑). Figs. 5c, d In the vicinity of the plasma membrane, either microapocrine secretion of membranous matrix vesicles (MV: d = 40–300 nm) or distribution and accumulation of collagen type I fibrils (∗: d = 25–40 nm, banding: 50–60 nm) extending towards the central ECM are observed. Fig. 5e In the central region of the intercellular ECM, distribution of Cellmatrix Type I-A collagen fibrils (■: thick fibrils d = 15–48 nm) with indistinct bandings (20 nm) is observed. Fig. 5f Calcification loci (↑) formation (1.0 × 1.0 ～ 2.0 × 5.0 μm^2) closely related with the Cellmatrix Type I-A collagen scaffold meshwork are observed.

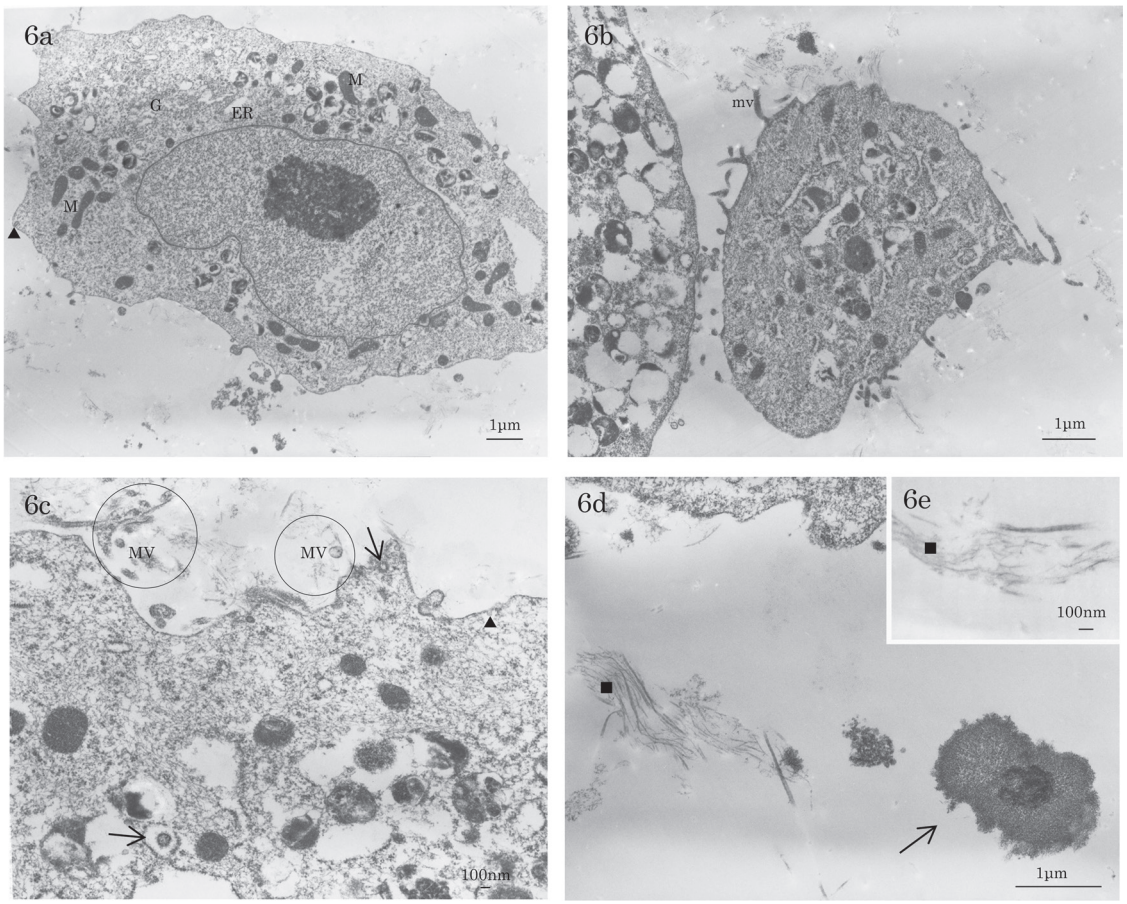

Fig. 6. TEM of the experimental group (day 7 experimentals). Figs. 6a, b The mature Ob-like HMS0014 cells extend cytoplasmic processes exhibiting structural surface modification of many microvilli (mv). In the cytoplasm, the endoplasmic reticulum (ER) and Golgi apparatus (G) are well developed. Many mitochondria (M) in longitudinal and cross sections showing orthodox configuration with condensed matrix are observed. Paraplasm of small smooth-surface vesicles (▲) distributed nearby/at the cell membrane is observed to be organelles providing for vesicular trafficking of the Ob-like cells. Fig. 6c Small smooth-surface vesicles (▲) distributing nearby/at the cell membrane, coated vesicles (↑), microapocrine secretion of MVs and mineralisation of the ECM (circled areas) are demonstrated. Figs. 6d, e The centre of the ECM is mainly distributed with Cellmatrix Type I-A collagen fibrils (■: d = 10–40 nm, band interval = indistinct to 20 nm); collagen-mediated mineralisation (d = 100–280 nm), and subsequent calcospherites and calcification loci (↑) formation closely related with the Cellmatrix meshwork are evident in TEM observations.

membrane, either microapocrine secretion of MVs (d = 40–300 nm) or distribution and accumulation of thin collagen type I fibrils (d = 25–40 nm, band interval = 50–60 nm) extending towards the central portion of the ECM were observed; MV- and subsequent collagen-mediated mineralisation adjacent to the Ob-like cells were demonstrated (Figs. 5c & 5d). In the centre of the ECM, about 2–5 μm distant from the neighboring cells, distribution of Cellmatrix Type I-A collagen fibrils (d = 15–48 nm) with indistinct fine band intervals (20 nm) was found; collagen-mediated mineralisation (d = 100–280 nm) and calcification loci formation (1.0 μm × 1.0 μm to 2.0 μm × 5.0 μm) closely related with the Cellmatrix Type I-A collagen scaffold meshwork were also found (Figs. 5b, 5e & 5f).

(2) Day 7 specimens:

The mature Ob-like HMS0014 cells (cell body size = 8 μm × 20 μm to 10 μm × 50 μm) extended cytoplasmic processes exhibiting structural surface modification of many microvilli (Figs. 6a & 6b). In the cytoplasm, the endoplasmic reticulum (ER) and Golgi apparatus were well developed. Many mitochondria in longitudinal and cross sections showing orthodox configuration with condensed matrix were also observed (Figs. 6a & 6b). Paraplasm of small smooth-surface vesicles distributed nearby/at the cell membrane were observed to be organelles providing for vesicular trafficking of the Ob-like cells (Figs. 6a, 6b & 6c). On the other hand, endocytosis mediated by formation of coated vesicles (r ≒ 180 nm, the upper area of the coated pit; d ≒ 400 nm) was also demonstrated in the cytoplasm; paraplasmic vesicles

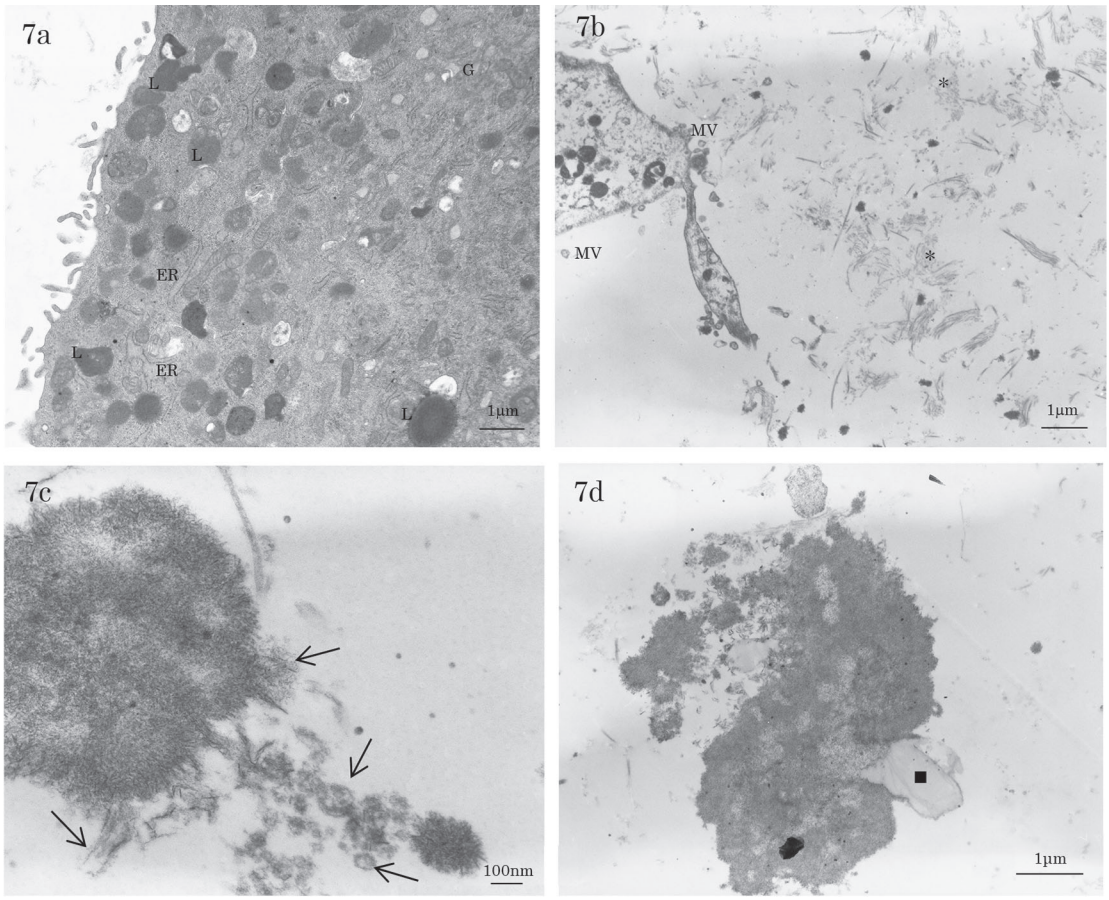

Fig. 7. TEM of the experimental group (day 14 experimentals). Fig. 7a TEM showing a mature Ob-like cell which extends many microvilli. The cytoplasm contains numerous organelles supporting vesicular transport/trafficking mechanisms (e.g., G, ER & L). Fig. 7b At the periphery of Ob-like cells, exocytosis (supposed to be related with the constitutive pathway), micro-apocrine secretory matrix vesicles (MV), and accumulation of collagen type I fibrils (*) are observed. Fig. 7c In the central ECM, TEM shows matrix vesicle-mediated mineralisation, collagen type I-mediated mineralisation and calcification loci (↑). Fig. 7d TEM showed collagen-mediated mineralisation of Cellmatrix Type I-A collagen fibres (■).

closely related with electron-dense lysosomes which were also characteristically abundant in the day 7 Ob-like cells (Fig. 6a, 6b & 6c).

It was near to the plasma membrane, MV- and collagen-mediated mineralisation arose spatially and structurally by the nucleation phenomena (Fig. 6a, 6c & 6d). On the other hand, the centre of the ECM were mainly distributed with Cellmatrix Type I-A collagen fibrils (d = 10–40 nm, band interval = indistinct to 20 nm); collagen-mediated mineralisation (d = 100–280 nm), and subsequent calcospherites and calcification loci formation were evident in TEM of the Cellmatrix meshwork (Fig. 6d & 6e).

(3) Day 14 specimens:

The day 14 HMS0014 cells cultured with Cellmatrix Type I-A showed similar TEM findings to the day 7 specimens; abundant cytoplasm distributed with well-developed morphoplasm accompanied with the presence of numerous lysosomes was identified to be the intracellular structures regulating vesicle traffic of the Ob-like cells (Fig. 7a). At the periphery of the cells, many vesicular budding of MVs and accumulation of collagen type I fibrils (d = 25–40 nm, band interval = 50–60 nm) were found. Furthermore, the occurrence of both matrix vesicle- and collagen-mediated mineralisation events adjacent to the Ob-like cells was demonstrated in the ECM (Figs. 7b & 7c).

The ECM was rich in collagen fibrils and calcification loci of different sizes (1.0 μm × 1.0 μm to 10 μm × 10 μm; Fig. 7b). In the central region of the ECM sealing the space between neighboring HMS0014 cells, MV-mediated mineralisation showing needle-like crystallite deposition, subsequent calcospherite formation and accretion (180 μm × 240 nm to 10 μm × 10 μm), and collagen-mediated mineralisation along Cellmatrix Type I-A fibres

forming calcification loci were found (Fig. 7d).

(4) Day 21 specimens:

The day 21 cells showed similar histology with the days 7 and 14 specimens; TEM observed that they were cells abundant in morphoplasm. However, some Ob-like cells with nuclear envelopes had the perinuclear cisternal space dilated and filled with condensed substance. The nucleus was morphologically characterized with disintegrating nucleolemma showing dilation of nuclear pores to envelop condensed chromatin and many autophagic vacuoles (Fig. 8a). The histology indicated that Ob-like cells in the day 21 growing tissue-engineered material were entering the terminal phase of autophagic degeneration, a type of non-apoptotic programmed cell death. GJS connecting degenerative cells and adjacent cells were evident (Figs. 8a & 8b). Exocytotic vesicles, as well as membranous MVs were demonstrated at the periphery cytoplasm and cell membrane (Fig. 8c). On the other hand, the fine structure examination showed that the ECM was abundantly distributed with bundles of collagen fibrils and calcification loci (Figs. 8d & 8e). The TEM also revealed MV- and Type I collagen-mediated calcification in the ECM; Cellmatrix Type I-A collagen fibrils were hardly identified in the day 21 specimens (Figs. 8d & 8e).

The day 21 osteogeneic-inducted Ob-like cells spread and were intercellularly connected with many fine cytoplasmic protrusions (Fig. 8a). In the abundant cytoplasm, it was rich in kinds of membranous organelles and ribosomes, and the cytosol was filled with a well-developed cytoskeletal network of microfilaments (d = 3–6 nm), intermediate filaments (d ≒ 10 nm) and microtubules (Figs. 8a, 8c, 8e & 8f).

Fluorescence IHC by LSM

The results were summarised and demonstrated the protein expression related with autophagic-lysosomal degeneration pathway and cell death signal conduction mediated with GJS of Ob-like bone-derived MSCs (Table 1; Figs. 9a & 9b, 10a & 10b).

1. LC3 autophagy-related protein expression

The autophagic vacuole marker protein LC3 was not immumolocalised in the day 3 controls (Fig. 9a). However, the expression of LC3 was evident in the days 3, 7, 14 and 21 experimental osteoproductive Ob-like cells (Fig. 9b).

2. Cx43 GJS protein expression

The GJS are type of surface domains essentially related with moderation of cell death, signal conduction and turnover of the Ob-like cells.

Cx43 expression was observed in HMS0014 cells of both the controls and experimentals (Fig. 10a). The LSM results indicated that the number of GJS between the adjacent Ob-like cells have increased over time of experiment (Fig. 10b).

The present fluorescence IHC by LSM indicated that there was autophagic-lysosomal degeneration pathway modified with cell death signal conducted of neighbouring Ob-like cells that maintained tissue homeostasis by regulating the life and death of the bone-derived MSCs in the growing peri-IP tissue-engineering material.

Discussion

Several studies on dental implant (IP) osseointegration have elucidated that peri-IP bone bonding began with osteoinduction allowing for attachment and subsequent differentiation of osteogeneic linage cells to initiate osteoconduction to facilitate the direct bone-to-implant contact (BIC) of IPs[3, 4, 6, 9, 12, 15, 18, 20–22, 29, 30, 34]. Nevertheless, the studies have emphasized that the development of focal contacts of the attached osteogeneic cells essentially mediated the IP surface substrate responses to affect cell spreading and signaling and thereby modified contact osteogenesis at the cell-substratum interface[1, 3, 4, 6, 12, 15, 19, 20, 35–39]. Previously, we have studied the histochemical properties (e.g., by ALPase activity, Ca volume, osteocalcin volume studies) and osteoconduction of mouse KUSA/A1 (JCRB/HSRRB) and human HMS0014 Yub621b (Riken BRC) osteogeneic linage MSCs in monolayer and 3D cultures, and then cultured the cells on titanium (Ti) discs with different surface substrates (i.e., anodic oxidation, hydroxyapatite coating, precision blasting). The results revealed that the immature bone-derived MSCs were condition-induced to actively proliferate, migrate and spread to acquire focal adhesions and intercellular connections with well-developed lamellipodia (extended sheet-like cytoplasmic protrusions supported with a meshwork of branched cytoskeletal proteins) and filopodia (finger-like protrusions supported with a parallel array of microfilaments assembled in long bundles) within 180 minutes, and were differentiated into mature osteoblast (Ob)-like cells during three days of culture; the SEM study observed that HMS0014 cells were more expansively adhered on the anodic-oxidized (AO) Ti discs. Furthermore, fluorescent immunomicroscopy findings revealed co-expression of F-actin (actin filament, a cytoskeleton protein) and CD51 (the αv/β3 integrin: ITGAV, an interfacing specific receptor protein) in the differentiated Ob-like cells [8,11].

The integrin family of cell adhesion receptor molecules found in cell anchoring junctions has been elucidated to be the trans-membrane linker (anchoring) protein which actively transducts signals across the plasma membrane by tying cytoskeletal protein anchors (e.g., actin filaments) to ECM proteins with focal adhesions[40, 41]. On the other hand, there have been studies of

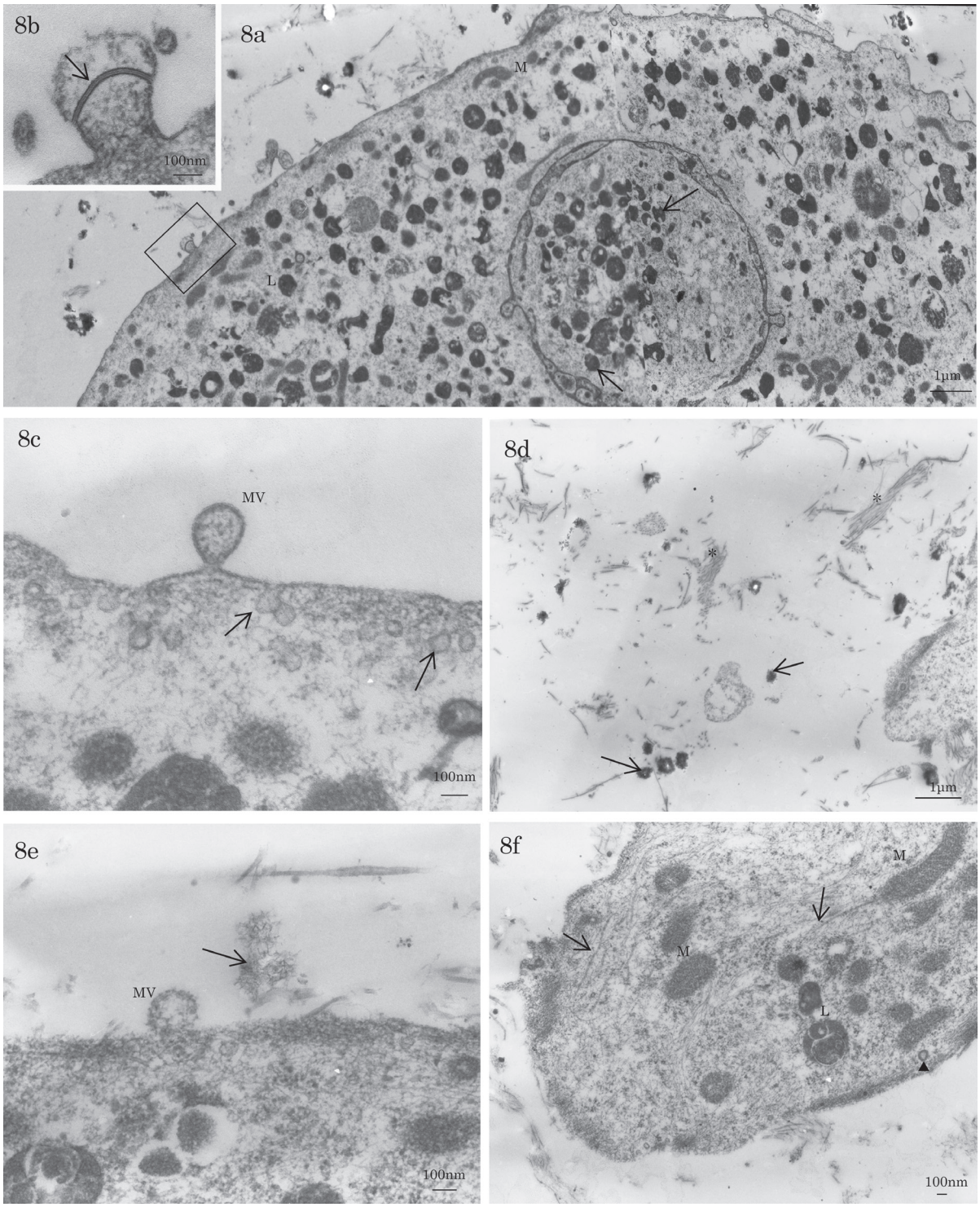

Fig. 8. TEM of the experimental group (day 21 experimentals). Fig. 8a The nucleolemma shows dilated nuclear pores and perinuclear cisternal space; the disintegrating nucleolamma envelopes many enlarged autophagic vacuoles (↑) (L: lysosome, M: mitochondrion). Fig. 8b The TEM shows the GJS (↑) connecting adjacent Ob-like cells. Fig. 8c Exocytotic vesicles (↑), as well as membranous MVs are demonstrated at the periphery cytoplasm and cell membrane. Figs. 8d, e The TEM shows that the ECM is abundantly distributed with bundles of collagen fibrils (∗) and calcification loci (↑). The TEM reveals MV- and Type I collagen-mediated calcification (↑) in the ECM; Cellmatrix Type I-A collagen fibrils are hardly identified in the day 21 specimens. Fig. 8f The day 21 cells are rich in kinds of membranous organelles (e.g., M: mitochondrion, L: lysosome, ▲: vesicle), ribosomes and a well-developed cytoskeletal network (↑).

LC3

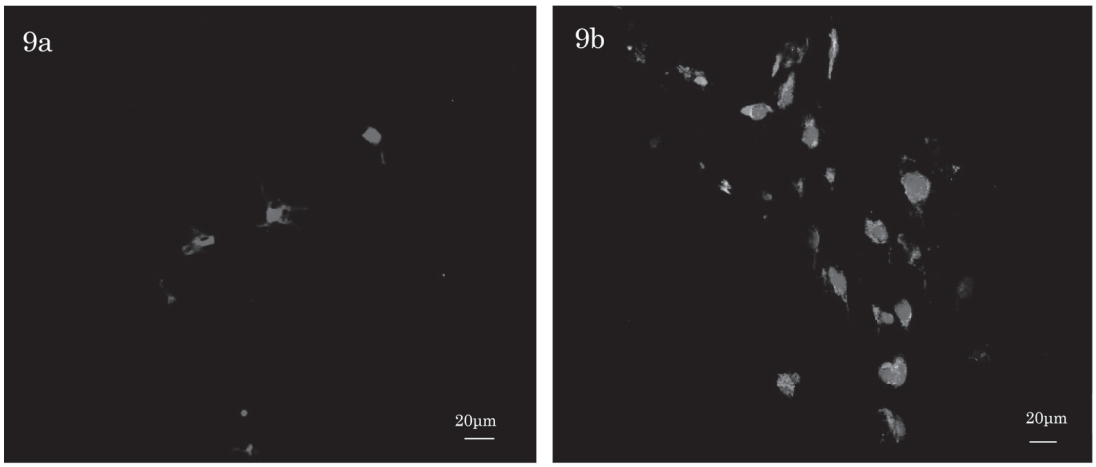

control (Day 3) experimental (Day 3)

Cx43

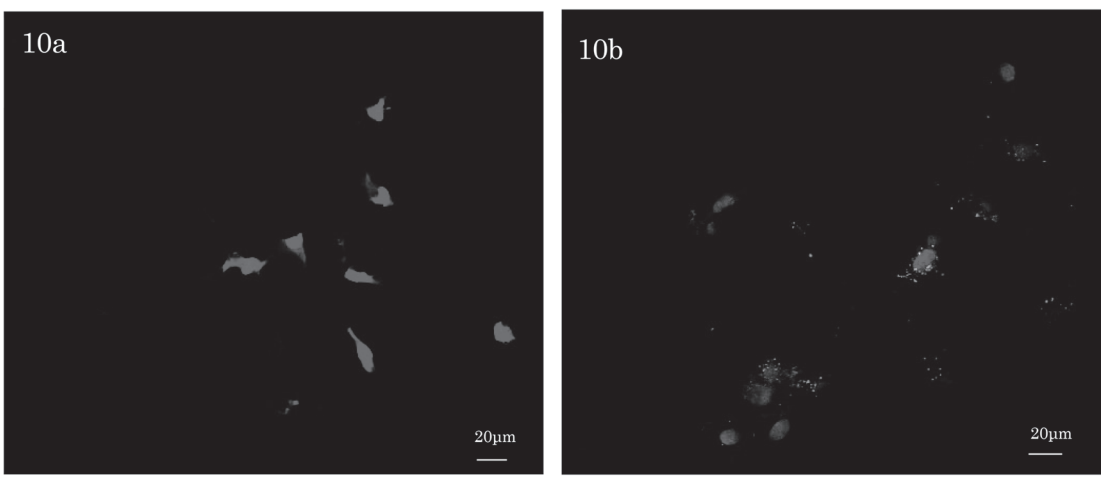

control (Day 3) experimental (Day 3)

Figs. 9 & 10. Fluoresence IHC by LSM. The LC3 autophagy-related protein and Cx43 GJS protein expression. The expression of autophagic vacuole marker protein LC3 expression and Cx43 GJS protein is not immumolocalised in the controls (Figs. 9a, 10a), but is evident in the experimental osteoproductive Ob-like cells (Figs. 9b, 10b) (represented by day 3 specimens).

Ob adhesion properties on biomaterials that elucidated the expression of integrin adhesion receptors involving in Ob-material interactions was essentially modified according to the surface characteristics of the biomaterials. The studies also elucidated that Obs would proliferate and differentiate into cells showing lamellipodia and filopodia with enhanced expression of F-actin filaments coupling with large focal contacts to adhere to the osteoinductive substratum; the IP surface substrate responses vice versa played active roles in events that governed not only osteoinduction (adherence and spreading, migration, proliferation, maturation and modulation of the Ob-like cells) but also the development of focal adhesion structures which mediated contact osteogenesis at the direct BIC interface[1, 3, 4, 6, 12, 15, 20, 35, 37–39, 42, 43]. In contrast, there has been a study demonstrating that inappropriate cell-matrix interactions might evoke signals transducted from type I collagen fibrils (e.g., of the ECM or scaffold) into surrounding cells through integrin, thereby inducing disoriented cell death to ensure the polarity of cells.

Table 1. Results

Protein expression	Fluorescence IHC by LSM				
	Control	Experimental			
	Day 3	Day 3	Day 7	Day 14	Day 21
LC3	–	+	+	+	+
Cx43	–	+	+	+	+

Alexa Fluor 488 goat anti-rabbit IgG [H + L] (excitation wavelength: 495 nm, fluorescence wavelength: 519 nm and PI DNA stain (excitation wavelength: 530 nm, fluorescence wavelength: 615 nm)

The study surmised that apoptosis played the important cell death mechanism in physiological developmental processes or under pathological conditions[42].

Some histological studies have indicated that certain chemical and physical signals occurring at the focal adhesions were transmitted to the cell body and subsequently shared with neighboring cells via intercellular junctions (e.g., adherence, gap junctional intercellular communication)[44–49]. On the other hand, the architecture of actin microfilamentous networks build up a F-actin cortex which was essential for the maintenance and regulation of cell shape and the generation of mechanical forces in cell migration, as well as the development of stress fibres to couple with focal adhesion plaques for transmission of forces towards the substrate and scaffolds[6, 42, 49]. Many other studies have elucidated that intracellular cytoskeletal elements were organised to be tension-bearing structures of beams (microtubules) and cables (micro- and intermediate filaments), giving structural support to hold and regulate cell shape by resisting buckling due to compressive forces and filament fracture, as well as a dynamic 3D structure to carry out cellular movements and convey information/signals about the microenvironment of the cells[6, 42, 49–51]. Our previous SEM studies have demonstrated that the actively proliferating and differentiating Ob-like HMS0014 cells adhered to and spread well on the surface of tested Ti discs and IPs under inducing conditions[11, 32]. In the present TEM study, we observed that the mature Ob-like HMS0014 cells contained many non-membranous cell organelles of microfilaments, intermediate filaments and microtubules in the cell body and peripheral cytoplasm. We speculated that the distribution of the F-actin cytoskeleton corresponds with the actin stress fibres, which have fibrillar ends co-localised with CD51 to represent focal adhesion formation of the HMS0014 cells under inducing conditions[11, 32].

The present TEM fine structure study revealed that the well-developed cytoskeleton and abundant membranous organelles seemed to be general characteristics of the mature Ob-like HMS0014 cells; a well-developed Golgi apparatus, rER, sER, polymorphic mitochondria in orthodox configuration containing dense matrix and other morphoplasm were evident in the cells. We also observed that distribution of coated vesicles and endosomes were spatially closely related with numerous electron-dense lysosomes, and identified vesicular transport and trafficking mechanisms of the osteoinducted cells[2, 52–54]. On the other hand, the changes in the number and size of mitochondria present in a cell are directly related to the cell's metabolic activity, and mitochondria undergo reversible ultrastructural transformations between a condensed and an orthodox conformation in relationship to either the osmotic balance between cytosol and the matrix or respiratory state of the cell. A previous study has elucidated that mitochondria with matrix of slow metabolite diffusion rate in the condensed state were dominant in a tissue with high level of oxidative phosphorylation[55]. However, it has been noted that the onset of phosphorylation was accompanied by a reduction of the matrix volume of orthodox mitochondria, but there is no evidence that the decrease in matrix volume affected the phosphorylation efficiency[56]. Nevertheless, other studies have reported that volume-dependent regulation of matrix protein packing may modulate metabolite diffusion and, in turn, mitochondrial metabolism of cells[57–59].

On the other hand, by TEM examination of the cell (top) layer as presented in this study, budding of paraplasm of small smooth-surface vesicles and formation of coated vesicles nearby/at the cell membrane, as well as accumulation of nascent/thin collagen type I fibrils and microapocrine secretion of MVs at the periphery of cell membrane in the ECM were demonstrated; we identified that the ECM contained hybrid of collagen secreted by Ob-like cells and distributed by the Cellmatrix Type I-A gel. Furthermore, the study revealed a temporo-spatial replacement of the finely divergent Cellmatrix networks by collagen type I fibrils secreted from Ob-like HMS0014 cells in the ECM; the Cellmatrix collagen fibrils were not evident in the cell layer of day 21 specimens. Meanwhile, it was similar to what has described for contact osteogenesis during osseointegration, we identified cement line formation at the periphery of Cellmatrix Type I-A fibres and fibrils in the cell layer. Collectively, we have elucidated osteoconduction of MSCs to commence MV- and collagen-mediated mineralisation in a collagenous 3D ECM scaffold to develop a tissue-engineering peri-IP osteoid tissue *in vitro*[2, 9, 13–19, 30, 32].

In the present study, LC3 localisation was used as a marker of autophagosome formation in the Ob-like cells of the tissue-engineered material[60]. The fluorescence IHC by LSM detected the expression of LC3 expression in experimental Ob-like cells. Meanwhile by using TEM for observation of Ob-like cells, we observed that day 21 experimentals had the nuclear enveloped with dilated perinuclear cisternal space filled with condense substance, and the nucleus was morphologically characterized with disintegrating nucleolemma showing dilation of nuclear pores to envelop condensed chromatin and many enlarged autophagic vacuoles. The histological studies observed that day 21 Ob-like cells in the growing GBR tissue were entering the terminal phase of non-apoptotic programmed cell death (PCD) -the type 2 physiological cell death showing autophagic degeneration-, thereby indicated immunohistochemical and ultrastructural evidence for progressive autophagic degeneration resulting in PCD of the Ob-likes cells in the GBR tissue[61, 62].

In addition, the present TEM and LSM observed that other than adherens junctions, the cells were connected by GJS for allowing the transmission of electrical impulses among their neighbouring cells. GJS have been elucidated to be channels playing an important function in maintaining cellular energy homeostasis and cell survival by spreading cell-killing signals initially generated by a single cell that spontaneously initiated apoptosis into healthy non-apoptotic neighbours. Thus, the GJS regulated important roles in the life and death of cells by moderating cell death signal conduction to migrate the bystander effect between contacting cells[51, 63–66]. Some studies have further stated that the recycling function of autophagy through a lysosomal degradation pathway was a decisive factor not causing the unaffected healthy bystander cells to also die and thereby maintained cellular energy homeostasis and survival. Moreover, PCD has been elucidated to be a self-limited survival strategy rather than a primary or irreversible death execution program[62, 67–69].

Tissue engineering for GBR by the placement of osteogeneic cells within matrices to recapitulate the development and formation of biological implantation tissue has been proposed to be a predictable strategy for a decrease in the need for recruitment of cells at the defect site[70–73]. Previously, we have *in vitro* studied osseointegration of a peri-IP tissue-engineered material by mouse KUSA/A1 bone marrow-derived MSCs cultured with Cellmatrix Type I-A Gel[9]. The GBR method engineered mouse osteogeneic MSCs in the 3D collagen networks to initiate contact osteogenesis at the cell-substrate interfaces followed with mineral apposition of the growing peri-IP tissue to acquire osteoid tissue which provided bone-to-implant direct contact (BIC) without intervening soft tissue at the interfaces[9, 12, 16, 30].

Taken together, in the present study by embedment of the AO-IP with cell clusters containing human osteogeneic HMS0014 Yub621b BMSCs in the Cellmatrix Type I-A Gel fashioned from natural material, we investigated histological events associated with growth of a biological tissue-engineered osseointegrative material to surround the dental IP[70–74]. Consequently, the TEM and LSM results elucidated that the active Ob-like HMS0014 cells contained the morphoplasm providing for the vesicular transport and trafficking mechanisms, as well as structures related with osteoconduction of the cells in osseointegration of Ti IPs. Moreover, we identified the LC3 autophagic gene expression and configuration of autophagy-mediated programmed cell death to maintain cellular energy homeostasis and cellular survival of the Ob-like cells distributed in the peri-IP mineralising tissue[62, 67, 68]. The study concluded that the present GBR method osteoinducted human bone-derived MSCs within a 3D ECM scaffold to actively regulate a homeostatic microenvironment for commencing osteoconduction of the peri-IP tissue *in vitro*. Furthermore, we surmised that the tissue-engineered osteoid tissue might be utilised as a supplementary material for the IP in the host drilled socket, thereby employs a biocompatible and biodegradable BIC tissue which would be remolded and modeled to optimize functional osseointegration for the endosseous implant therapy[9, 75–77].

Acknowledgements

This work was partly supported by a grant-in-aid for scientific research (C) (24592976) from the Ministry of Education, Culture, Sports, Science, and Technology of Japan. The human mesenchymal stem cells line, HMS0014 (Yub621b), was provided by the RIKEN BRC through the National Bio-Resource Project of the MEXT, Japan. The study was performed using the Laboratory Animal, Morphological Research and Tissue Culture Facilities in the Institute of Dental Research, Osaka Dental University. The study results were presented at the 56th Annual Meeting of Japanese Association for Oral Biology in Fukuoka on September 27, 2014.

References

1) Anselme K. Osteoblast adhesion on biomaterials. *Biomaterials* 2000; **21:**667–681.
2) Albrektsson T, Johansson C. Osteoinduction, osteoconduction and osseointegration. *Eur Spine J* 2001; **10** (Suppl 2): S96–101.
3) Boyan BD, Lossdörfer S, Wang L, Zhoa G, Lohmann CH, Cochran DL, Schwartz Z. Osteoblasts generate an osteogenic microenvironment when growth on surfaces with rough microtopographies. *Eur Cell Mater* 2003; **6:**22–27.
4) Nasatzky E, Gultchin J, Schwartz Z. The role of surface roughness in promoting osteointegration. *Refuat Hapeh Vehashinayim* 2003; **20:**8–19, 98.
5) Diener A, Nebe B, Lüthen F, Becker P, Beck U, Neumann HG,

Rychly J. Control of focal adhesion dynamics by material surface characteristics. *Biomaterials* 2005; **26:**383–392.
6) Salido M, Vilches Jl, Gutiérrez JL, Vilches J. Actin cytoskeletal organization in human osteoblasts grown on different dental titanium implant surfaces. *Histol Histopathol* 2007; **22:**1355–1364.
7) Ferguson SJ, Langhoff JD, Voelter K, von Rechenberg B, Scharnweber D, Bierbaum S, Schnabelrauch M, Kautz AR, Frauchinger VM, Mueller TL, van Lenthe GH, Schlottig F. Biomechanical comparison of different surface modifications for dental implants. *Int J Oral Maxillofac Implants* 2008; **23:**1037–1046.
8) Nakatsuka M, Mikami T, Hashimoto Y, Kon-I H, Chen HS, Hsiao SY, Kumabe S, Huang ST, Iwai Y, Huang HC. A preliminary study of osseointegration in the dental implant therapy *in vivo* —culture of mouse KUSA/A1 cells on titanium plates with different surface modifications—. *TWJ Oral Med Sci* 2009; **25:**4–19.
9) Mikami T, Kumabe S, Y Iwai. A study of osseointegration -3D culture of KUSA/A1 cells with a collagen scaffold on titanium implants with different surface modifications. *J Oral Tissue Engin* 2010; **8**:60–73.
10) Nakatsuka M, Hashimoto Y, Kumabe S, An C, Ueda K, Mikami H, Huang HC, Iwai Y. The study of cell attachment and hard tissue formation on the dental implant surface [Abstract]. *Kaibougaku Zasshi* 2010; **85** (Suppl): 177. (in Japanese)
11) Iwai Y, Matsuda Y, Nakatsuka M, Mikami Y, Kumabe S. A preliminary study of the dental implant therapy —initial osteogenesis of human mesenchymal stem (HMS0014) cells on titanium discs with different surface modifications—. *Okajimas Folia Anat Jpn* 2012; **88:**133–140.
12) Davies JE. *In vitro* modeling of the bone/implant interface. *Anat Rec* 1996; **245:**426–445.
13) Murai K, Takeshita F, Ayukawa Y, Kiyoshima T, Suetsugu T, Tanaka T. Light and electron microscopic studies of bone-titanium interface in the tibiae of young and mature rats. *J Biomedical Mater Res* 1996; **30:**523–533.
14) Rosengren A, Johansson BR, Danielsen N, Thomsen P, Ericson LE. Immunohistochemical studies on the distribution of albumin, fibrinogen, fibronectin, IgG and collagen around PTFE and titanium implants. *Biomaterials* 1996; **17:**1779–1786.
15) Davies JE. Mechanisms of endosseous integration. *Intl J Prosthodont* 1998; **11**:391–401.
16) Puelo DA, Nanci A. Understanding and controlling the bone-implant interface. *Biomaterials* 1999; **20:**2311–2321.
17) Ferretti M, Palumbo C, Contri M, Marotti G. Static and dynamic osteogenesis: Two different types of bone formation. *Anat Embryo*l 2002; **206**:21–29.
18) Davies JE. Understanding peri-implant endosseous healing. *J Dent Educ* 2003; **67:**932–949.
19) Marco F, Milena F, Gianluca G, Vittoria O. Peri-implant osteogenesis in health and osteoporosis. *Micron* 2005; **36:**630–644.
20) Grössner-Schreiber B, Tuan RS. Die Bedeutung der Oberfläche von Titaniimplantaten in Osteointegrationvorgang (The influence of the titanium implant surface on the process of osseointegration). *Dtsch Zanhartzl Z* 1991; **46**:691–693.
21) Meyer U, Büchter A, Wiesmann HP, Joos U, Jones DB. Basic reactions of osteoblasts on structured material surfaces. *Eur Cell Mater* 2005; **9:**39–49.
22) Issac J, Loty S, Hamdan A, Kokubo T, Kim HM, Berdal A, Sautier JM. Bone-like tissue formation on a biomimetic titanium surface in an explant model of osteoconduction. *J Biomed Mater Res A* 2009; **89:**585–593.
23) Holmes TC. Novel peptide-based biomaterial scaffolds for tissue engineering. *Trend Biotechnol* 2002; **20:**16–21.
24) Kisiday J, Jin M, Kurz B, Hung H, Semino C, Zhang S, Grodzinsky AJ. Self-assembling peptide hydrogel fosters chondrocyte extracellular matrix production and cell division: implications for cartilage tissue repair. *Proc Natl Acad Sci USA* 2002; **99:**9996–10001.
25) Zhang S. Fabrication of novel biomaterials through molecular self assembly. *Nat Biotechnol* 2003; **21:**1171–1178.
26) Kisiday JD, Jin M, DiMicco MA, Kurz B, Grodzinsky AJ. Effects of dynamic compressive loading on chondrocyte biosynthesis in self-assembling peptide scaffolds. *J Biomech* 2004; **37:**595–604.
27) Bokhari MA, Akay G, Zhang S, Birch MA. The enhancement of osteoblast growth and differentiation *in vitro* on a peptide hydrogel- polyHIPE polymer hybrid material. *Biomaterials* 2005; **26:**5198–5208.
28) Fillies T, Wiesmann HP, Sommer D, Joos U, Meyer U. Osteoblast reaction on SLA and microgroved implant surfaces. *Mund Kiefer Gesichtschir* 2005; **9:**24 –28.
29) Inoue T. Mechanisms of metabolism and wound healing. In: Yamazaki M, Takahashi T, Katsuyama H, Inoue T, Hayashi Y, eds, *The Ultimate Guide to Implant Dentistry.* Tokyo, Japan: Ishiyaku Publishers Inc.; 2004: 38–53.(in Japanese)
30) Inoue T. Histology (Bone Soft tissue). In: Akagawa Y et al., eds. *Fundamental concepts and techniques of oral implants.* 2nd ed. Tokyo, Japan: Ishiyaku Publishers, Inc.; 2005: 40–60.(in Japanese)
31) Koyano K, Matsushita Y, Ayukawa Y. Basic science for the dental implantology. In: Koyano K, Matsuura M, eds. *Essential oral implantology*. Tokyo, Japan: Ishiyaku Publishers, Inc.; 2009: 10–17.(in Japanese)
32) Iwai Y, Mikami Y, Nakatsuka M, Huang HC, Mikami H, Kumabe S. A preliminary study of the dental implant therapy —initial osteogenesis of human mesenchymal stem (HMS0014) cells on titanium discs and implants with different surface modifications—. *J Tissue Eng Regen Med* 2012; **6 (Suppl. 1):** 234–235.
33) Mohammad AAY, Asai J. Ultrastructural and morphometrical studies on the reticular framework and reticular fibers in the reticuloendothelial system of rats. *Nagoya J Med Sci* 1993; **55:**47–56.
34) Joos U, Meyer U. New paradigm in implant osseointegration. *Head Face Med* 2006; **2:**19.
35) Lange R, Lüthen F, Beck U, Rychly J, Baumann A, Nebe B. Cell-extracellular matrix interaction and physico-chemical characteristics of titanium surfaces depend on the roughness of the material. *Biomol Eng* 2002; **19**:255–261.
36) Jayaraman M, Meyer U, Bühner M, Joos U, Wiesmann HP. Influence of titanium surfaces on attachment of osteoblast-like cells *in vitro*. *Biomaterials* 2004; **25:**625–631.
37) Lenhert S, Meier MB, Meyer U, Chi L, Wiesmann HP. Osteoblast aligment, elongation and migration on grooved polystyrene surfaces patterned by Langmuir-Blodgett lithography. *Biomaterials* 2005; **26:**563–570.
38) Graf HL, Stoeva S, Armbruster FP, Neuhaus J, Hilbig H. Effect of bone sialoprotein and collagen coating on cell attachment to TICER and pure titanium implant surfaces. *Int J Oral Maxillofac Surg* 2008; **37:**634–640.
39) Coelho PG, Granjeiro JM, Romanos GE, Suzuki M, Silva NR, Cardaropoli G, Thompson VP, Lemons JE. Basic research methods and current trends of dental implant surface. *J Biomed Mater Res B Appl Biomater* 2009; **88:**579–596.
40) Albert B, Johnson A, Lewis J, Raff M, Roberts K, Walter P. *Molecular Biology of the Cell.* 4th edition. New York, NY: Garland Science; 2002:1–29.
41) Stricker J, Falzone T, Gardel ML. Mechanics of the F-actin cytoskeleton. *J Biomechanics* 2010; **43:**9–14.
42) Lim JY, Taylor AF, Li Z, Vogler EA, Donahue HJ. Integrin expression and osteopontin regulation in human fetal osteoblastic cells mediated by substratum surface characteristics. *Tissue Eng* 2005; **11:**19–29.
43) Tang MJ, Hu JJ, Lin HH, Chiu WT, Jiang ST. Collagen gel overlay induces apoptosis of polarized cells in cultures: disoriented cell death. *Am J Physiol* 1998; **275**:C921–931.
44) Rosendaal M, Green CR, Rahman A, Morgan D. Up-regulation of the connexin43+ gap junction network in haemopoietic tissue before the growth of stem cells. *J Cell Sci* 1994; **107:**29–37.

45) Shapiro F. Variable conformation of GAP junctions linking bone cells: a transmission electron microscopic study of linear, stacked linear, curvilinear, oval, and annular junctions. *Calcif Tissue Int* 1997; **61:**285–293.
46) Donahue HJ. Gap junctions and biophysical regulation of bone cell differentiation. *Bone* 2000; **26:**417–422.
47) Chen CS, Alonso JL, Ostuni E, Whitesides GM, Ingber DE. Cell shape provides global control of focal adhesion assembly. *Biochem Biophys Res Commun* 2003; **307:**355–361.
48) Yap AS, Kovacs EM. Direct cadeherin-activated cell signalling: a view from the plasma membrane. *J Cell Biol* 2003; **160:**11–16.
49) Lim JY, Donahue HJ. Biomaterial characteristics important to skeletal tissue engineering. *J Musculoskelet Neuronal Interact* 2004; **4:**396–398.
50) Guo Y, Martinez-Williams C, Rannels DE. Gap junction-microtubule associations in rat alveolar epithelial cells. *Am J Physiol Lung Cell Mol Physiol* 2003; **285:** L1213-L1221.
51) Lu JG, Sun YN, Wang C, Jin DJ, Liu M. Role of the αv-integrinin subunit in cell proliferation, apoptosis and tumor metastasis of laryngeal and hypopharyngeal squamous cell carcinomas: a clinical and in vitro investigation. *Eur Arch Otorhinolaryngol* 2009; **266:**89–96.
52) Thyberg J, Friberg U. Electron microscopic enzyme histochemical studies on the cellular genesis of matrix vesicles in the epiphyseal palate. *J Ultrastruct Res* 1972; **41:**43–59.
53) Nimura A, Egawa K. High resolution scanning electron microscopy of formative bone surface by endochondral ossification. *J Showa Univ Dent Soc* 1985; **5:**118–126.(in Japanese)
54) Watanabe T, Sakai Y, Hira Y, Bochimoto H, Hosaka M. Molecular and cellular basis for the secretory granule biogenesis in endocrine cells. *Microscopy* 2008; **43:**29–34.(in Japanese)
55) Kassik A, Safiulina D, Zharkosky A, Veksler V. Regulation of mitochondrial matrix volume. *Am J Physiol Cell Physiol* 2007; **292:**C157–C163.
56) Lang RD, Bronk JR. A study of rapid mitochondrial structural changes in vitro by spary-freeze-etching. *J Cell Biol* 1978; **77:**134–147.
57) Scalettar BA, Abney JR, Hackenbrock CR. Dynamics, structure, and function are coupled in the mitochondrial matrix. *Proc Natl Acad Sci USA* 1991; **88:**8057–8061.
58) Gottlieb E, Armour SM, Harris MH, Thompson CB. Mitochondrial membrane potential regulates matrix configuration and cytochrome c release during apoptosis. *Cell Death and Differ* 2003; **10:**700–717.
59) Dąbrowska E, Balunowska M, Letko R, Szynaka B. Ultrastructural study of the mitochondria in the submandibular gland, the pancreas and the liver of young rats, exposed to NaF in drinking water. *Rocz Akad Med Bialymst* 2004; **49** Suppl 1:180–181.
60) Martinet W, De Meyer GR, Andries L, Herman AG, Kockx MM. Detecttion of autophagy in tissue by standard immunohistochemistry: possibilities and limitations. *Autophagy* 2006; **2:**55–57.
61) Mizushima N. Methods for monitoring autophagy. *Int J Biochem Cell Biol* 2004; **36:**2491–2502.
62) Kitanaka C. Non-apoptotic programmed cell death: existence and significance of programmed cell deaths having morphology and mechanism distinct from apoptosis. *Yamagata Med J* 2005; **23:**83–96.
63) Mesnil M, Piccoli C, Triraby G, Willecke K, Yamasaki H. Bystander killing of cancer cells by herpes simplex virus thymidine kinase gene is mediated by connexions. *Proc Natl Acad Sci USA* 1996; **93:**1831–1835.
64) Krutovskikh VA, Piccoli C, Yamasaki H. Gap junction intercellular communication propagates cell death in cancerous cells. *Oncogene* 2002; **21:**1989–1999.
65) Frank DK, Szymkowiak B, Josifovska-Chopra O, Nakashima T, Kinnaly KW. Single-cell microinjection of cytochrome *c* can result in gap junction-mediated apoptotic cell death of bystander cells in head and neck cancer. *Head Neck* 2005; **27:**794–800.
66) Wang CM, Lincoln J, Cook JE, Becker DL. Abnormal connexin expression underlies delayed wound healing in diabetic skin. *Diabetes* 2007; **56:**2809–2817.
67) Bi WL, Parysek LM, Warnick R, Stambrook PJ. In vitro evidence that metabolic cooperation is responsible for the bystander effect observed with HSV tk retroviral gene therapy. *Hum Gene Ther* 1993; **4:**725–731.
68) Levine B, Yuan JY. Autophagy in cell death: an innocent convict? *J Clin Invest* 2005; **115:**2679–2688.
69) Apel A, Zentgraf H, Büchler MW, Herr I. Autophage- A double-edged sword in oncology. *Intl J Cancer* 2009; **125:**991–995.
70) Langer R, Vacanti J. Tissue engineering. *Science* 1993; **260:**920–926.
71) Bartold PM, McCulloch C, Narayanan AS, Pitaru S. Tissue engineering: A new paradigm for periodontal regeneration based on molecular and cell biology. *Periodontol 2000* 2000; **24:**253–269.
72) Hämmerle C, Jung RE. Bone augmentation by means of barrier membranes. *Periodontol 2000* 2003; **33:**36–53.
73) Sparks MS, Kerns DG, Wilson TG, Hallmon WW, Spears R, Haghighat N. Bone regeneration around implants in the canine mandible with cultured fibroblasts in polyglactin mesh. *J Periodontol* 2007; **78:**1276–1287.
74) Paolantonio M, Dolci M, Scarano A, d' Archivio D, di Placido G, Turnini V, Piattelli A. Immediate implantation in fresh extraction sockets. A controlled clinical and histological study in man. *J Periodontol* 2001; **72:**1560–1571.
75) Hoshaw SJ, Brunski JB, Cochran GVB. Mechanical loading of Brånemark implants affects interfacial bone modeling and remodelling. *Intl J Oral Maxillofac Implants* 1994; **9:**345–360.
76) Skedros JG, Mason MW, Bloebaum RD. Modeling and remodeling in a developing artiodactyl calcaneus: a model for evaluating Frost's mechanostat hypothesis and its corollaries. *Anat Rec* 2001; **263:**167–185.
77) Seeman E. Bone modeling and remodeling. *Crit Rev Eukaryot Gene Expr* 2009; **19:**219–233.